Desalination and Water Treatment
www.deswater.com

doi: 10.5004/dwt.2022.28309

254 (2022) 251–259
April

Calcination effects on sol–gel preparation of porous TiO_2/zeolite composites for Acid Red 1 degradation

Minghua Wang, Wenjie Zhang*, Yingjie Tao, Lili Yang

School of Environmental and Chemical Engineering, Shenyang Ligong University, Shenyang 110159, China, emails: wjzhang@aliyun.com (W. Zhang), 1261291548@qq.com (M. Wang), 2995910063@qq.com (Y. Tao), 1925415193@qq.com (L. Yang)

Received 28 August 2021; Accepted 16 February 2022

ABSTRACT

A sol–gel synthesizing method was applied to prepare thin porous titanium dioxide layer supported on the zeolite. Hexadecyltrimethylammonium bromide can enhance the porosity of TiO_2 layer and the activity. This work aims at the influences of calcination temperature on the characteristics of the TiO_2/zeolite composites. The only substance in the supported layer of the TiO_2/zeolite composites is anatase TiO_2. The crystallite sizes of anatase titanium dioxide in the composites calcined at 350°C, 400°C, 450°C and 500°C are 8.8, 10.0, 11.8 and 12.3 nm, and the bandgap energies are 2.67, 3.08, 3.21 and 3.21 eV for the composites, respectively. The TiO_2/zeolite composites are typical mesoporous materials, and the mesopores are formed in the TiO_2 layer. The composite sample calcined at 400°C has the largest specific surface area (229.7 m^2/g), which is close to that of the zeolite. Many mesopores are formed in the TiO_2 layer of the TiO_2/zeolite composite. The maximum number of hydroxyl radical is produced on the TiO_2/zeolite composite calcined at 400°C, accompanied with the strongest photocatalytic activity. Acid Red 1 dye is almost thoroughly degraded after 90 min of reaction in the presence of the TiO_2/zeolite composite.

Keywords: Photocatalytic degradation; Sol–gel; TiO_2; Hexadecyltrimethylammonium bromide; Acid Red 1

1. Introduction

The concern of hazardous organic pollutants has promoted the wastewater treatment techniques [1]. The wastewater treatment techniques include the traditional flocculation, adsorption and biochemical treatments. The photocatalytic oxidation of organic pollutants has become a prospective technique in wastewater treatment [2,3]. Many harmful organic substances, for example, industrial dyes and antibiotics, can be degraded by the photocatalytic oxidation technique, and fully mineralization of these organic pollutants can be accomplished [4–6]. Numerous literatures about the application of titanium dioxide were reported [7–10]. Modification of the material is necessary to fulfill the operation conditions in the treatment plants [11–15].

Fine photocatalyst particles usually have a large surface area and good activity, but the fine particles are easily suspended in the wastewater. Since the materials are reused after wastewater treatment, the materials must be quickly removed from the water. Photocatalyst films are deposited on glass, ceramic and other kinds of substrates [16–20]. Although the supported photocatalyst films can be easily removed from the water, the activity of the films is usually much weaker than the activity of the fine particles. HZSM-5 zeolite is studied as a porous supporting material, and the most interesting finding is the improved photocatalytic activity of the supported TiO_2 [21–23].

Templates are used to synthesize porous photocatalysts, and the activity of the materials usually depends on the porous structure [24–26]. The influences of a template on the

* Corresponding author.

1944-3994/1944-3986 © 2022 Desalination Publications. All rights reserved.

supported TiO_2 are interesting, especially if the support is also a porous zeolite. In the present work, hexadecyltrimethylammonium bromide was applied to prepare the zeolite supported titanium dioxide via a sol–gel route. The photocatalytic activity of the TiO_2/zeolite composites was compared using Acid Red 1.

2. Experimental details

2.1. Material synthesis

HZSM-5 zeolite (SiO_2/Al_2O_3 = 25) is a kind of man-made zeolite (Nankai Catalyst Corporation, China). Hydrochloric acid (0.1 mL) and anhydrous ethanol (12 mL) were mixed with 2 mL of tetrabutyl titanate to prepare a solution, and then the zeolite, 3 g of hexadecyltrimethylammonium bromide (HTAB) and 0.9 mL of water were mixed with the solution. The obtained gel was dehydrated at 110°C, followed by 3 h of calcination. The TiO_2/zeolite composites has a TiO_2: zeolite weight ratio of 3:7.

2.2. Characterization of the composites

The morphology images of the TiO_2/zeolite materials were obtained using an accelerating voltage of 15 kV (Quanta 250). The phase composition of the TiO_2/zeolite composites was examined using an D8 X-ray diffractometer. A G2 transmission electron microscope (TEM) was used for the high-resolution image. The infrared spectra of the TiO_2/zeolite materials were obtained using a spectrometer. The diffuse reflectance spectra were obtained using a UV-Vis spectrometer (LAMBDA 35). A 2460 analyser was applied to obtain the pore size and surface area of the composites.

2.3. Photocatalytic reactions

The TiO_2/zeolite composites were evaluated by the removal of Acid Red 1 azo dye. The dye solution (40 mg/L, 50 mL) and the composite powders (30 mg TiO_2) were stirred in a quartz beaker in the dark until the Acid Red 1 concentration was stable. The 253.7 nm photons were emitted by a 20 W lamp to initiate Acid Red 1 degradation. A spectrophotometer (721E) was used to determine Acid Red 1 concentration. Terephthalic acid was the reactant to indicate the generation of hydroxyl radicals.

3. Results and discussion

3.1. Surface morphology

Fig. 1 gives the surface morphologies of the TiO_2/zeolite composites, TiO_2 and the zeolite. The very large TiO_2 particles of approximately several tens of micrometers in the size are formed in the TiO_2 sample (Fig. 1e), due to the aggregation of the sol–gel synthesized TiO_2 crystals. Fig. 1a–d show the TiO_2/zeolite materials prepared at different calcination temperatures. 30% TiO_2 is supported on 70% zeolite in the composites. Some regular zeolite particles can be seen in the images, but the surface of the particles is much rougher than the pure zeolite particles. Large TiO_2 particles are not in the composites, because TiO_2 crystals aggregation is prohibited in the supported TiO_2 layer [21,22]. Fig. 2 presents the TEM high resolution image of the TiO_2-zeolite boundary in the TiO_2/zeolite composite calcined at 400°C. The nano-sized titanium dioxide crystals are tightly adhered to the zeolite. The crystal size of anatase TiO_2 is approximately 10 nm, and the thickness of TiO_2 layer is less than 100 nm.

3.2. Composition of the composites

Fig. 3 presents the diffraction patterns of the TiO_2/zeolite composites. The strong diffraction peaks of the zeolite situated at 2θ = 8.0°, 8.9°, 23.2° and 24.3° are found in the diffraction patterns of the composites [27]. The TiO_2 in the TiO_2/zeolite is in anatase TiO_2 phase (JCPDS 01-562). Since TiO_2 weight percent in the composites is only 30%, the X-ray diffraction (XRD) intensity of anatase titanium dioxide is not strong. The crystallization of anatase TiO_2 occurs at relatively low calcination temperature, and the crystals slightly grow up at higher calcination temperature. The TiO_2 crystallite sizes in the composites calcined at 350°C, 400°C, 450°C and 500°C are 8.8, 10.0, 11.8 and 12.3 nm, respectively. The nano-sized anatase TiO_2 crystals are produced in all the TiO_2/zeolite composites, even though the calcination temperature is as high as 500°C.

Fig. 4 presents the infrared spectra of the TiO_2/zeolite composites. The zeolite has a strong absorption band centered at 1,092 cm^{-1} for the Al(Si)–O bonds [28,29]. The absorption at 543 cm^{-1} is for the Si–O–Al pentagon ring [30]. The absorptions at 796 and 1,221 cm^{-1} are for the Al–O–Al or Si–O–Si bonds [30]. The Ti–O bonds have two absorptions situated at 446 and 343 cm^{-1} [31]. Organic residues are also in the TiO_2/zeolite composites, showing by the peaks at 2,926 and 2,853 cm^{-1}. The composites were calcined below 500°C in this work, and the organic substances were not thoroughly removed from the materials. The hydroxyl groups on the material surface have two strong absorption bands at 3,429 and 1,638 cm^{-1}.

3.3. Bandgap energy of the TiO_2/zeolite composites

As shown in Fig. 5a, the absorption edges of the TiO_2/zeolite composite are in the visible–ultraviolet radiation boundary (380–420 nm). The zeolite is an insulator so that the zeolite does not absorb irradiation in this region. Therefore, the absorption edges of the materials indicate the characteristic of the supported TiO_2. The bandgap energies were calculated using $(\alpha h\nu) = A(h\nu - E_g)^n$, that is, the Tauc-plot method [32]. The $h\nu$–$(ah\nu)^2$ plots are illustrated in Fig. 5b. The bandgap energies are 2.67, 3.08, 3.21 and 3.21 eV for the materials prepared at 350°C, 400°C, 450°C and 500°C, respectively. It is known that anatase TiO_2 has the bandgap energy of approximately 3.2 eV. The bandgap energies of the composites calcined at 450°C and 500°C are almost the same to the typical bandgap energy of anatase TiO_2. The increased absorption for the composites calcined below 400°C is due to the unburned organic residues.

3.4. Porous properties

The adsorption–desorption isotherms are shown in Fig. 6a to identify the porous properties of the TiO_2/zeolite composites. The N_2 isotherms can be explained by the

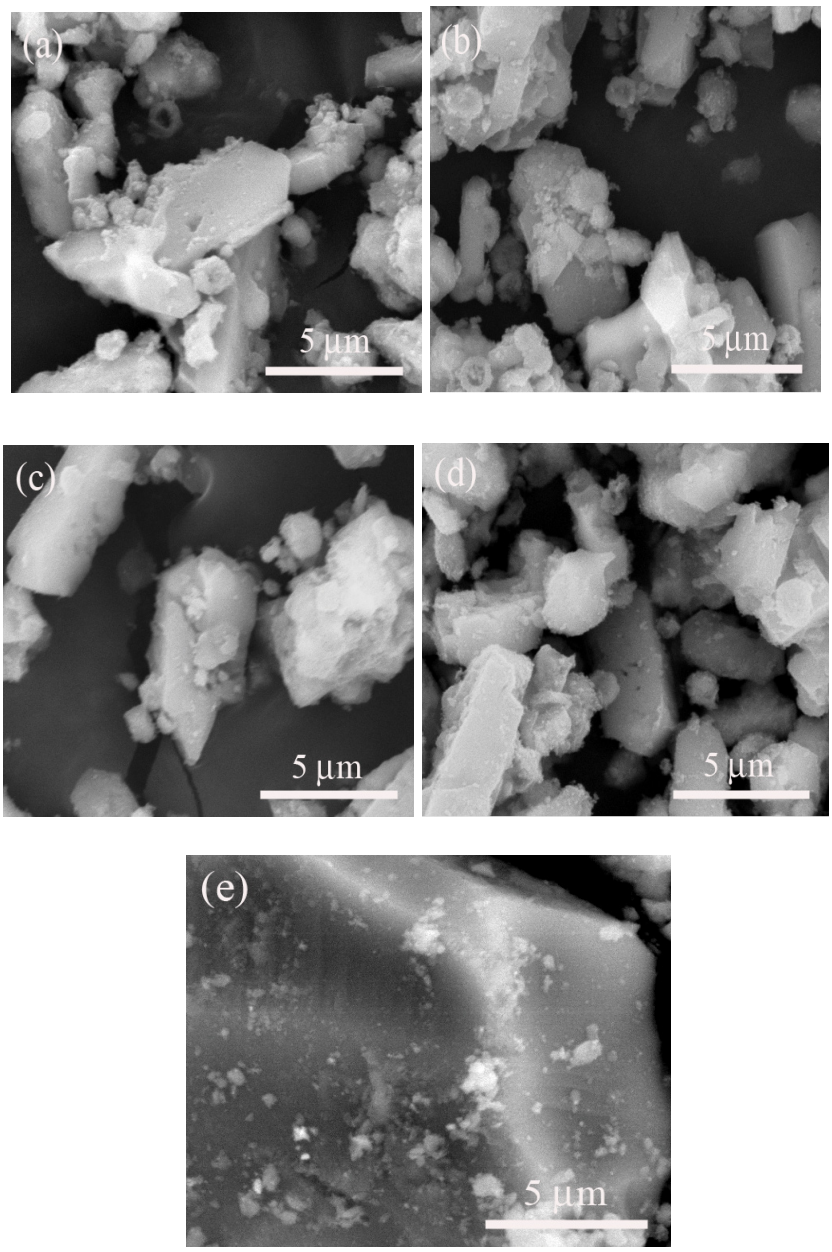

Fig. 1. Scanning electron microscopy (SEM) images of TiO_2/zeolite composites calcined at 350°C (a), 400°C (b), 450°C (c) and 500°C (d); SEM image of (e) TiO_2.

characteristics of both the zeolite and TiO_2. Gaseous N_2 molecules are adsorbed on the composites at low N_2 partial pressure (normally below 0.3). The pores in the composites are filled with liquefied nitrogen when N_2 partial pressure is larger than 0.3. The number of adsorbed N_2 molecules slightly increases in the partial pressure range between 0.2 and 0.6. The abrupt increase of adsorbed nitrogen occurs at higher partial pressure, and this is caused by nitrogen condensation in the mesopores and the macropores in the materials.

The isotherms of the TiO_2/zeolite composites have a hysteresis loop (type H1) as the nitrogen partial pressure range is between 0.6 and 0.9. The type IV isotherm indicates a mesoporous characteristic of the composites. The mesopores must be formed in the supported TiO_2 layer. Calcination temperature influences the quantity of adsorbed N_2 molecules on the TiO_2/zeolite composites. The composite calcined at 350°C can adsorb the smallest number of N_2 molecules. The adsorbed N_2 quantity increases with rising calcination temperature until the largest N_2 molecules are adsorbed on the composite calcined at 450°C. However, the adsorbed N_2 quantity on the composite calcined at 500°C obviously decreases. Calcination temperature can influence both anatase TiO_2 crystallization and porous structure of the composites. This will be discussed in details later.

The mesopore size distributions in the TiO_2/zeolite composites are shown in Fig. 6b. The mesopores in the

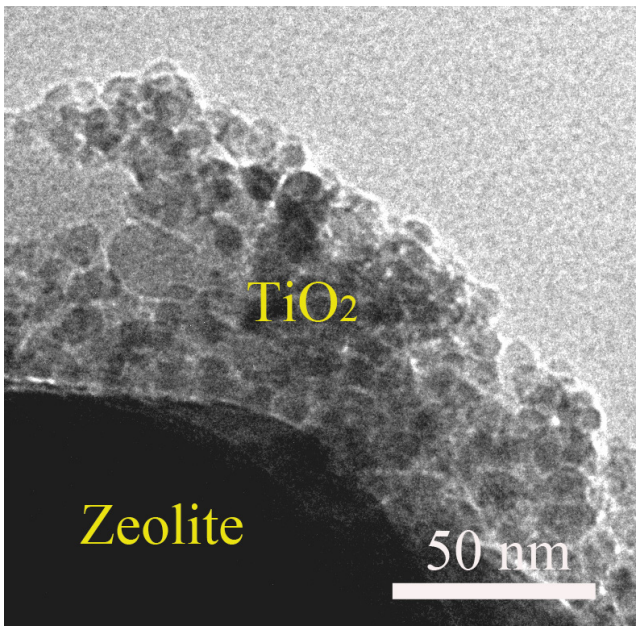

Fig. 2. TEM image of the TiO_2/zeolite composite calcined at 400°C.

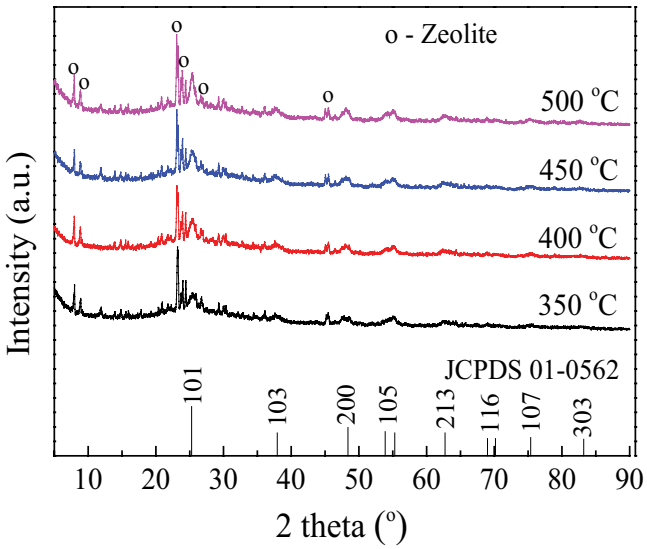

Fig. 3. XRD patterns of the TiO_2/zeolite composites.

composites are enlarged at higher calcination temperature, and the pore volumes are also enlarged. All the mesopores in the composites are in the size below 20 nm. Fig. 6c indicates the micropores and Fig. 6d shows the micropore surface area of the composites. The micropore volumes of the composites are much smaller than the mesopore volumes, but the micropores can provide large surface areas. Most of the micropores in the TiO_2/zeolite composites are in the zeolite, and the zeolite nearly has no mesopores.

Table 1 lists the pore volume and the surface area of the materials. The specific surface area of the zeolite (233.2 m^2/g) is greater than those of the composites, but the pore volume in the zeolite (0.121 cm^3/g) is smaller than those of the composites. The differences must be due to the TiO_2 in the composites, while calcination temperature can obviously influence these properties.

The TiO_2/zeolite composite calcined at 350°C has the smallest specific surface area, that is, 145.0 m^2/g, due to incomplete crystallization of titanium dioxide, and the micropores in the zeolite might be occupied by some unburned substances. The TiO_2/zeolite composite calcined at 400°C has the largest value of 229.7 m^2/g, which is very close to the value of the zeolite. This sample has the largest pore volume as well. Many mesopores are formed in the TiO_2 layer of the TiO_2/zeolite composite. Along with the removal of organic substances during calcination process, the micropores in the zeolite are also exposed. On the other hand, crystal growth at higher calcination temperature also leads to the shrinkage of both the pore volume and the surface area. The enlarged surface area is due to the supported

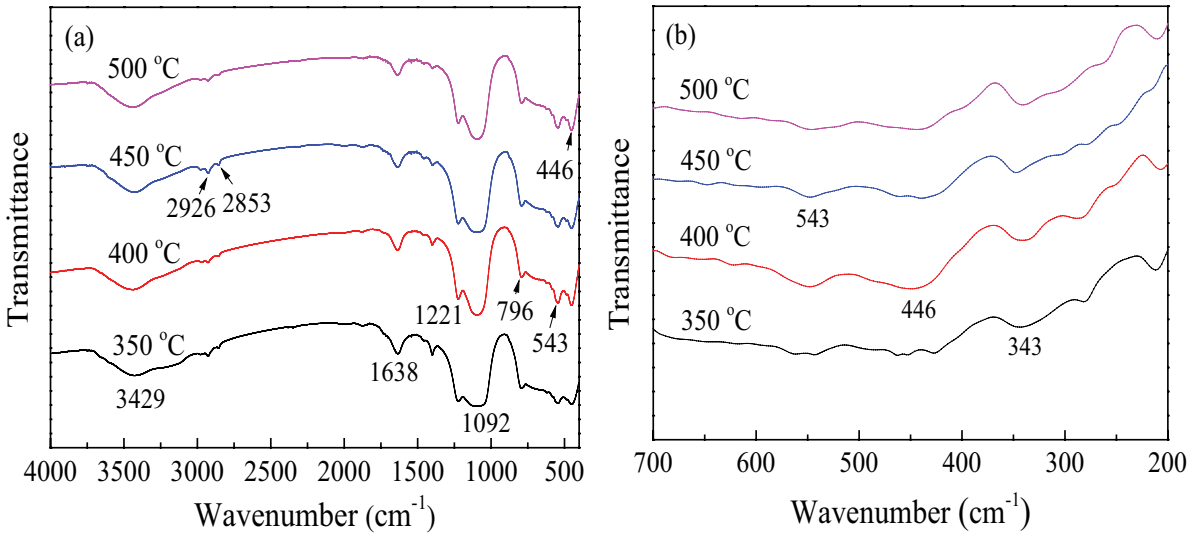

Fig. 4. Fourier-transform infrared spectra of the TiO_2/zeolite composite.

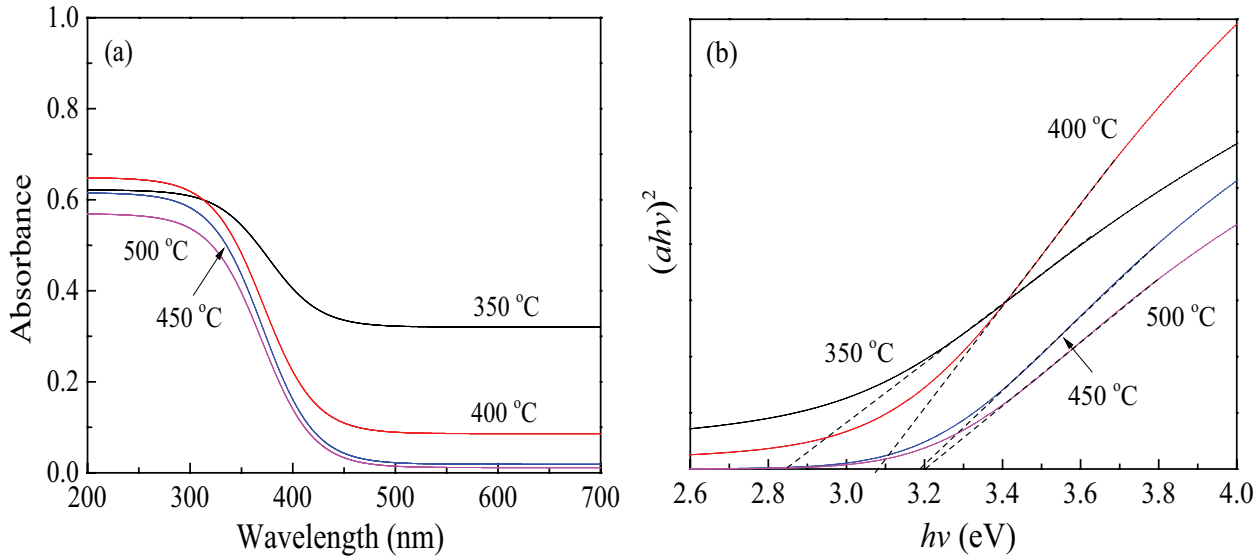

Fig. 5. (a) UV-Vis reflectance spectra of the TiO_2/zeolite composites and (b) $h\nu$–$(\alpha h\nu)^2$ plots.

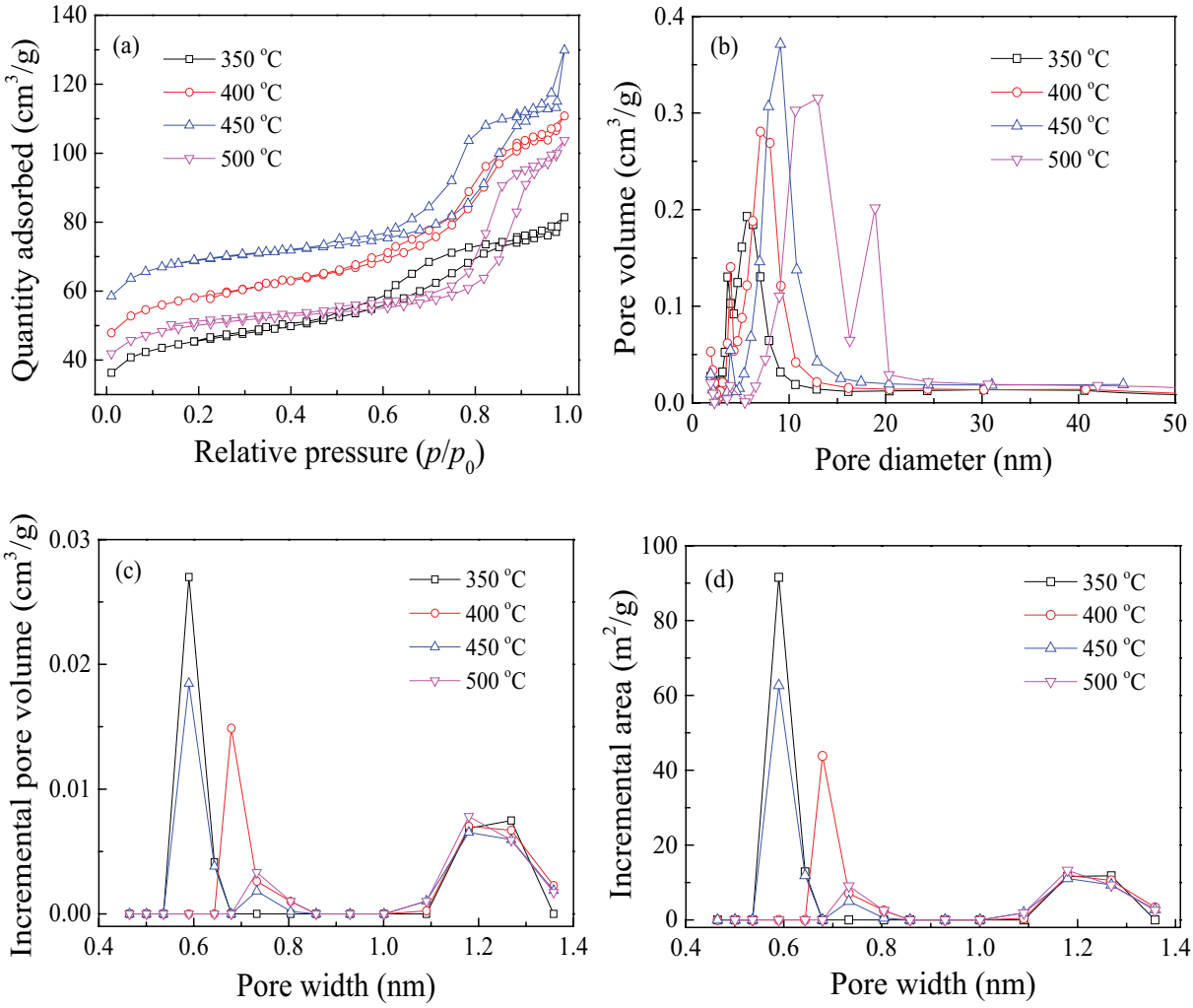

Fig. 6. (a) Adsorption–desorption isotherms (N_2) of the composites, (b) and (c) mesopore and micropore sizes, and (d) micropore surface area.

Table 1
The pore volume and surface area of the TiO_2/zeolite composites

Calcination temperature (°C)	Brunauer–Emmett–Teller surface area (m^2/g)	Micropore surface area (m^2/g)	Other surface area (m^2/g)	Pore volume (cm^3/g)
350	145.0	88.0	57.0	0.119
400	229.7	161.8	67.9	0.175
450	213.6	157.9	55.7	0.173
500	156.6	109.4	47.2	0.149

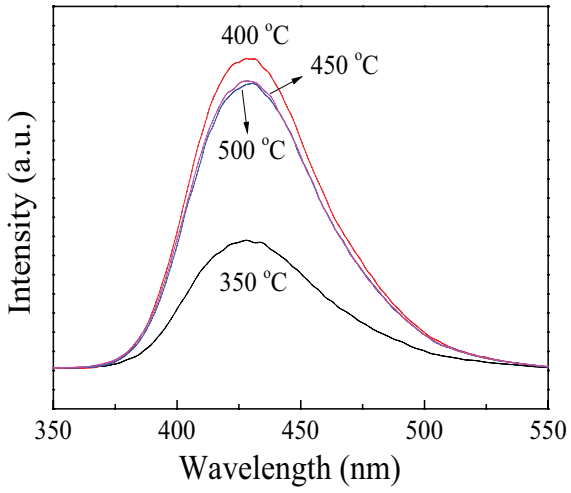

Fig. 7. Fluorescence spectra after 30 min of UV illumination on the 2-hydroxyterephthalic acid solution containing the TiO_2/zeolite composites.

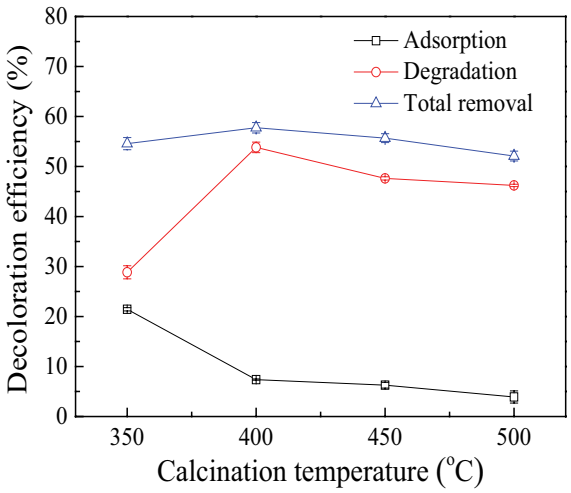

Fig. 8. Acid Red 1 removal on the TiO_2/zeolite composites. The reaction time was 30 min.

TiO_2, including the external surface of the TiO_2 and the surface of mesopores in the composites.

3.5. Hydroxyl radical production

The hydroxyl radicals produced in the reaction are indicated by the oxidation of terephthalic acid. Terephthalic acid is oxidized by hydroxyl radical to produce 2-hydroxyterephthalic acid. Since 2-hydroxyterephthalic acid may emit fluorescence after excitation, the hydroxyl radicals can be identified by the fluorescence intensity of the 2-hydroxyterephthalic acid solution. The fluorescence spectra of the solution after UV excitation are shown in Fig. 7. The fluorescence intensity is related to the number of hydroxyl radicals generated under illumination. The TiO_2/zeolite composite calcined at 400°C has the strongest power to produce hydroxyl radicals, and this composite might have strong photocatalytic activity.

3.6. Removal of azo dye

The performance of the TiO_2/zeolite composites is evaluated using photocatalytic decomposition of Acid Red 1. Fig. 8 shows the removal efficiencies in the presence of the composites. More than 20% of the dye molecules are adsorbed on the TiO_2/zeolite composite calcined at 350°C. When the calcination temperature is raised from 400°C to 500°C, the adsorbed Acid Red 1 molecules decrease from 7.4% to 3.9%. The carbon residues can be removed during high temperature calcination process, leading to the sharp decline of the adsorbed azo dye molecules. Another reason might be the shrinkages of both the pore volume and the surface area of the composites.

Both of the adsorption of Acid Red 1 and the photocatalytic decomposition occur on the composites. The dye molecules might enter the pores in the composites, but the degradation can only occur on the external surface of the materials. The TiO_2/zeolite composite calcined at 350°C has the weakest activity on dye degradation because of the insufficient crystallization of anatase titanium dioxide. The TiO_2/zeolite composite calcined at 400°C has the strongest photocatalytic activity, while further calcination temperature increment leads to a slight decline in the activity. The activity of the composites depends on anatase TiO_2 crystallization. However, slight crystal growth at higher calcination temperature might have a negative effect. Meanwhile, the activity of TiO_2/zeolite composites has an obvious relationship with the Brunauer–Emmett–Teller surface area.

Fig. 9a presents the decomposition of Acid Red 1 in the whole photocatalytic reaction. The Acid Red 1 molecules are continuously degraded with extended reaction time. Nearly all of the Acid Red 1 molecules are decomposed in 90 min in the presence of the TiO_2/zeolite composite calcined at 400°C. The reaction rate constants are 1.30×10^{-2},

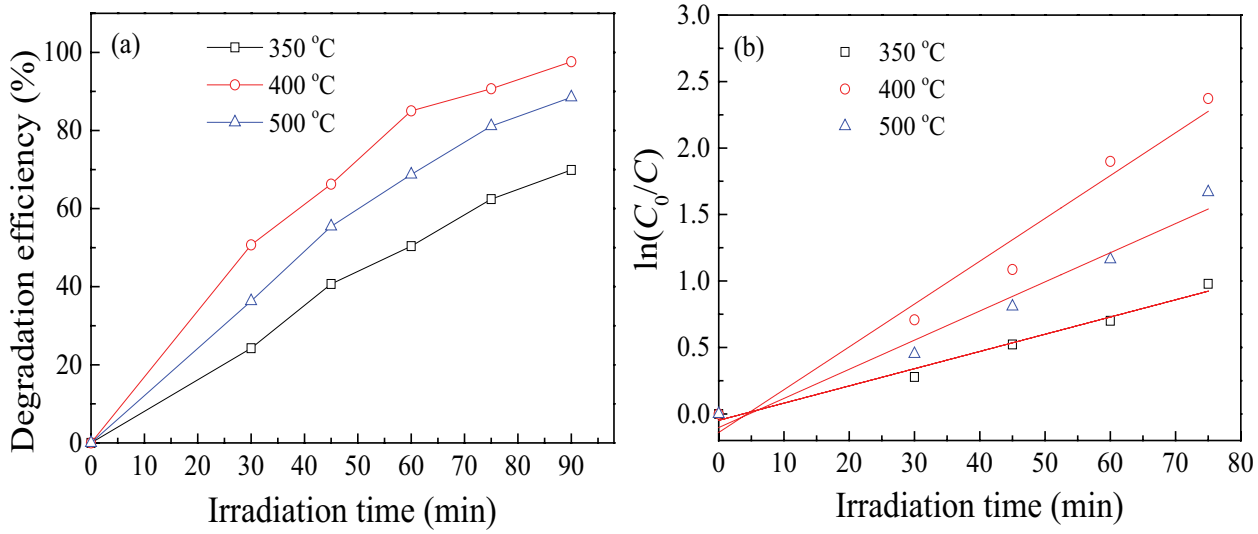

Fig. 9. (a) Decomposition of Acid Red 1 during illumination and (b) kinetic plots.

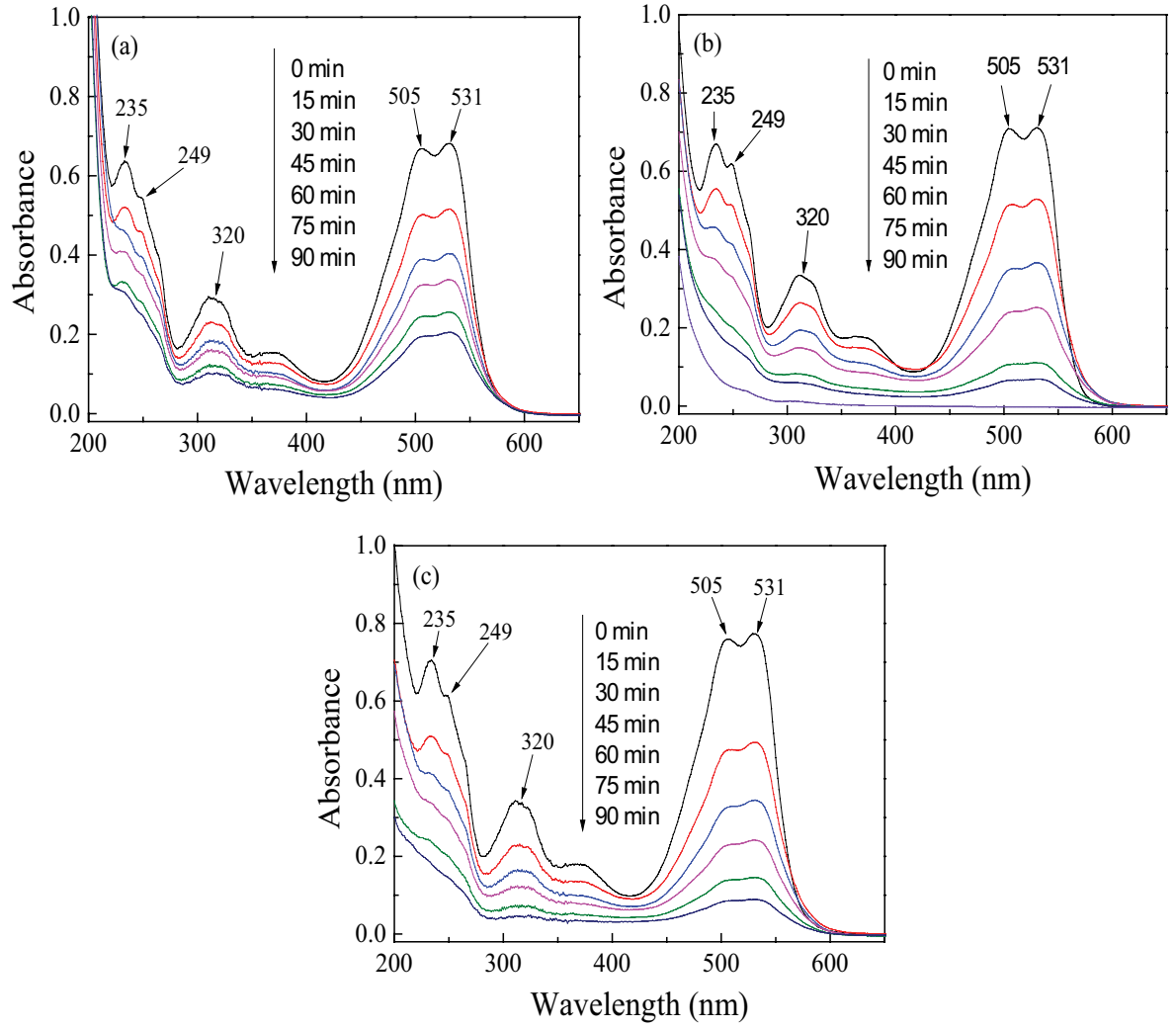

Fig. 10. UV-Vis absorption during Acid Red 1 degradation on the TiO_2/zeolite composites prepared at 350°C (a), 400°C (b), and 500°C (c).

3.22×10^{-2} and 2.19×10^{-2} min^{-1} for the materials prepared at 350°C, 400°C and 500°C, respectively, as shown in the kinetic plots in Fig. 9b.

Fig. 10 shows the light absorption of the azo dye solution in the photocatalytic reaction. The strong absorption band between 460–580 nm is due to the chromophore group of the dye. Three absorptions at 320, 249, and 235 nm are related to benzene ring and naphthalene ring, and the absorption peaks shrink with extended reaction time, depending on the activity of the TiO_2/zeolite. Acid Red 1 is almost thoroughly degraded after 90 min in the presence of the TiO_2/zeolite composite calcined at 400°C. The remaining solution has no absorption above 280 nm.

4. Conclusions

The porous TiO_2/zeolite composites were prepared by sol–gel method, using HTAB template in the sol–gel precursor. Calcination temperature can influence both anatase TiO_2 crystallization and porous structure in the composites. The nano-sized anatase TiO_2 crystals are bonded on the zeolite. The bandgap energies of the composites prepared at 450°C and 500°C are almost as same as the typical value of anatase titanium dioxide. Mesopores are formed in the TiO_2 layer of the TiO_2/zeolite composite. Nearly all the azo dye is decomposed in 90 min in the presence of the TiO_2/zeolite composite calcined at 400°C.

Acknowledgements

This work was supported by the Construction project of research innovation group of Shenyang Ligong University (SYLUTD202108).

References

[1] Q. Huang, C. Wang, D. Hao, W. Wei, L.C. Wang, B.-J. Ni, Ultralight biodegradable 3D-g-C_3N_4 aerogel for advanced oxidation water treatment driven by oxygen delivery channels and triphase interfaces, J. Cleaner Prod., 288 (2021) 125091, doi: 10.1016/j.jclepro.2020.125091.

[2] D. Barceló, B. Žonja, A. Ginebreda, Toxicity tests in wastewater and drinking water treatment processes: a complementary assessment tool to be on your radar, J. Environ. Chem. Eng., 8 (2020) 104262, doi: 10.1016/j.jece.2020.104262.

[3] D. Hao, Q. Huang, W. Wei, X.J. Bai, B.J. Ni, A reusable, separation-free and biodegradable calcium alginate/g-C_3N_4 microsphere for sustainable photocatalytic wastewater treatment, J. Cleaner Prod., 314 (2021) 128033, doi: 10.1016/j.jclepro.2021.128033.

[4] H.B. Lu, Y. Yu, Y.X. Zhou, F. Xing, A quantitative evaluation method for wastewater toxicity based on a microbial fuel cell, Ecotoxicol. Environ. Saf., 183 (2019) 109589, doi: 10.1016/j.ecoenv.2019.109589.

[5] W.T. Zhao, Q. Sui, X. Huang, Removal and fate of polycyclic aromatic hydrocarbons in a hybrid anaerobic-anoxic-oxic process for highly toxic coke wastewater treatment, Sci. Total Environ., 635 (2018) 716–724.

[6] M. Ma, Y. Liu, Y. Wei, D. Hao, W. Wei, B.J. Ni, A facile oxygen vacancy and bandgap control of $Bi(OH)SO_4 \cdot H_2O$ for achieving enhanced photocatalytic remediation, J. Environ. Manage., 294 (2021) 113046, doi: 10.1016/j.jenvman.2021.113046.

[7] S.L. Wang, S.H. Lin, D.Q. Zhang, G.S Li, M.K.H. Leung, Controlling charge transfer in quantum-size titania for photocatalytic applications, Appl. Catal., B, 215 (2017) 85–92.

[8] S. Deepracha, A. Ayral, M. Ogawa, Acceleration of the photocatalytic degradation of organics by *in-situ* removal of the products of degradation, Appl. Catal., B, 284 (2021) 119705, doi: 10.1016/j.apcatb.2020.119705.

[9] D.M. Tobaldi, D. Dvoranová, L. Lajaunie, N. Rozman, B. Figueiredo, M.P. Seabra, A. Sever Škapin, J.J. Calvino, V. Brezová, J.A. Labrincha, Graphene-TiO_2 hybrids for photocatalytic aided removal of VOCs and nitrogen oxides from outdoor environment, Chem. Eng. J., 405 (2021) 126651, doi: 10.1016/j.cej.2020.126651.

[10] V. Likodimos, Photonic crystal-assisted visible light activated TiO_2 photocatalysis, Appl. Catal., B, 230 (2018) 269–303.

[11] M. Ateia, M.G. Alalm, D. Awfa, M.S. Johnson, C. Yoshimura, Modeling the degradation and disinfection of water pollutants by photocatalysts and composites: a critical review, Sci. Total Environ., 698 (2020) 134197, doi: 10.1016/j.scitotenv.2019.134197.

[12] Y. Zhao, Y. Wang, G. Xiao, H. Su, Fabrication of biomaterial/TiO_2 composite photocatalysts for the selective removal of trace environmental pollutants, Chin. J. Chem. Eng., 27 (2019) 1416–1428.

[13] C. Gong, C.Z. Jiang, Preparation of nickel oxide under magnetic field strengthening conditions and its photocatalytic activity, J. Shenyang Ligong Univ., 39 (2020) 46–51.

[14] M.J. Torralvo, J. Sanz, I. Sobrados, J. Soria, C. Garlisi, G. Palmisano, S. Çetinkaya, S. Yurdakal, V. Augugliaro, Anatase photocatalyst with supported low crystalline TiO_2: the influence of amorphous phase on the activity, Appl. Catal., B, 221 (2018) 140–151.

[15] Q.Z. Gao, F.Y. Si, S.S. Zhang, Y.P. Fang, X.B. Chen, S.Y. Yang, Hydrogenated F-doped TiO_2 for photocatalytic hydrogen evolution and pollutant degradation, Int. J. Hydrogen Energy, 44 (2019) 8011–8019.

[16] S. Sharma, V. Dutta, P. Singh, P. Raizada, A. Rahmani-Sani, A. Hosseini-Bandegharaei, V.K. Thakur, Carbon quantum dot supported semiconductor photocatalysts for efficient degradation of organic pollutants in water: a review, J. Cleaner Prod., 228 (2019) 755–769.

[17] C. Prasad, Q. Liu, H. Tang, G. Yuvaraja, J. Long, A. Rammohan, G.V. Zyryanov, An overview of graphene oxide supported semiconductors based photocatalysts: properties, synthesis and photocatalytic applications, J. Mol. Liq., 297 (2020) 111826, doi: 10.1016/j.molliq.2019.111826.

[18] A. Juma, I. Oja Acik, A.T. Oluwabi, A. Mere, V. Mikli, M. Danilson, M. Krunks, Zirconium doped TiO_2 thin films deposited by chemical spray pyrolysis, Appl. Surf. Sci., 387 (2016) 539–545.

[19] G. Jagan Mohini, G. Sahaya Baskaran, V. Ravi Kumar, M. Piasecki, N. Veeraiah, Bioactivity studies on TiO_2-bearing Na_2O–CaO–SiO_2–B_2O_3 glasses, Mater. Sci. Eng., C, 57 (2015) 240–248.

[20] X.N. Lu, B.Z. Tian, F. Chen, J.L. Zhang, Preparation of boron-doped TiO_2 films by autoclaved-sol method at low temperature and study on their photocatalytic activity, Thin Solid Films, 519 (2020) 111–116.

[21] W.J. Zhang, F.F. Bi, Y. Yu, H.B. He, Phosphoric acid treating of ZSM-5 zeolite for the enhanced photocatalytic activity of TiO_2/HZSM-5, J. Mol. Catal. A: Chem., 372 (2013) 6–12.

[22] W.J. Zhang, K.L. Wang, Y. Yu, H.B. He, TiO_2/HZSM-5 nano-composite photocatalyst: HCl treatment of NaZSM-5 promotes photocatalytic degradation of methyl orange, Chem. Eng. J., 163 (2010) 62–67.

[23] P. Guo, X.S. Wang, H.C. Guo, TiO_2/Na-HZSM-5 nano-composite photocatalyst: reversible adsorption by acid sites promotes photocatalytic decomposition of methyl orange, Appl. Catal., B, 90 (2009) 677–687.

[24] N. Venkatachalam, M. Palanichamy, B. Arabindoo, V. Murugesan, Alkaline earth metal doped nanoporous TiO_2 for enhanced photocatalytic mineralisation of bisphenol-A, Catal. Commun., 8 (2007) 1088–1093.

[25] N. Arconada, A. Duran, S. Suárez, R. Portela, J.M. Coronado, B. Sanchez, Y. Castro, Synthesis and photocatalytic properties of dense and porous TiO_2-anatase thin films prepared by sol–gel, Appl. Catal., B, 86 (2009) 1–7.

[26] Y.H. Ao, J.J. Xu, D.G. Fu, C.W. Yuan, Preparation of porous titania thin film and its photocatalytic activity, Appl. Surf. Sci., 255 (2008) 3137–3140.

[27] Y. Sang, H.S. Li, Effect of phosphorus and mesopore modification on the HZSM-5 zeolites for n-decane cracking, J. Solid State Chem., 271 (2019) 326–333.
[28] H. Znad, K. Abbas, S. Hena, M.R. Awual, Synthesis a novel multilamellar mesoporous TiO_2/ZSM-5 for photo-catalytic degradation of methyl orange dye in aqueous media, J. Environ. Chem. Eng., 6 (2018) 218–227.
[29] A. Kostyniuk, D. Key, M. Mdleleni, Effect of Fe-Mo promoters on HZSM-5 zeolite catalyst for 1-hexene aromatization, J. Saudi Chem. Soc., 23 (2019) 612–626.
[30] D.D. He, Y.T. Zhao, S. Yang, Y. Mei, J. Yu, J.P. Liu, D.K. Chen, S.F. He, Y.M. Luo, Enhancement of catalytic performance and resistance to carbonaceous deposit of lanthanum (La) doped HZSM-5 catalysts for decomposition of methyl mercaptan, Chem. Eng. J., 336 (2018) 579–586.
[31] X.T. Zhang, G.W. Zhou, J. Xu, G.W. Bai, L. Wang, Synthesis and photocatalytic activity of co-doped mesoporous TiO_2 on Brij98/CTAB composite surfactant template, J. Solid State Chem., 183 (2010) 1394–1399.
[32] M.A. Butler, Photoelectrolysis and physical properties of the semiconducting electrode WO_2, J. Appl. Phys., 48 (1977) 1914–1920.